Neoplasma 2021; 68(4): 798–809

doi:10.4149/neo_2021_201206N1319

Depletion of circRNA circ_CDK14 inhibits osteosarcoma progression by regulating the miR-520a-3p/GAB1 axis

Peng-Fei WU[1], Xiao-Ming TANG[1], Hai-Lang SUN[1], Hai-Tao JIANG[1], Jian MA[1], Ying-Hui KONG[2,*]

[1]Department of Orthopedics, The Affiliated Huai'an No.1 People's Hospital of Nanjing Medical University, Huai'an, Jiangsu, China; [2]Department of Dermatology, The Affiliated Huai'an No.1 People's Hospital of Nanjing Medical University, Huai'an, Jiangsu, China

**Correspondence: hayygwk2020@163.com*

Received December 6, 2020 / Accepted April 7, 2021

Osteosarcoma (OS) is a lethal bone malignancy. Circular RNAs (circRNAs) have emerged as important regulators of OS development. CircRNA cyclin dependent kinase 14 (circ_CDK14) was reported to be a potential oncogene in OS. However, the mechanistic pathway by which circ_CDK14 functions in OS is largely unknown. The relative expression of circ_CDK14, microRNA (miR)-520a-3p, and GRB2 Associated Binding Protein 1 (GAB1) was evaluated by quantitative real-time PCR and western blot assays. Flow cytometry was employed to monitor cell cycle distribution and apoptosis. Methyl thiazolyl tetrazolium (MTT) and colony formation assays were performed to assess cell viability and colony formation ability, respectively. Western blot assay was also used to detect the expression of apoptosis-related proteins. Transwell assay was carried out to monitor cell migration and invasion. Additionally, the target association between miR-520a-3p and circ_CDK14 or GAB1 was confirmed by a dual-luciferase reporter assay. Xenograft assay was applied to investigate the role of circ_CDK14 *in vivo*. Circ_CDK14 and GAB1 expression was upregulated, while miR-520a-3p was downregulated in OS tissues and cells. Circ_CDK14 depletion hindered OS cell proliferation, metastasis, and tumorigenesis while facilitated apoptosis, which were all ameliorated by miR-520a-3p inhibition. Circ_CDK14 could sponge miR-520a-3p. miR-520a-3p targeted GAB1 to repress OS cell proliferation and metastasis. Circ_CDK14 knockdown blocked OS tumor growth *in vivo*. Circ_CDK14 might positively affect OS development by modulating the miR-520a-3p/GAB1 axis.

Key words: osteosarcoma, circ_CDK14, miR-520a-3p, GAB1, development

Osteosarcoma (OS) ranks as the most frequent bone tumor, which mainly attacks long bones in the limbs [1]. Taking up 2.4% of childhood cancers, OS is the eighth most common cancer among children [2]. Recently, highly advanced surgical techniques and chemotherapy have reduced the mortality rate and improved the prognosis of OS patients [3]. However, the 5-year survival of OS patients with metastasis is relatively low with only 20–28% [4]. Therefore, it's necessary to fully understand the molecular mechanism of OS, so as to develop potential therapeutic targets.

Circular RNAs (circRNAs) are a category of specific non-coding RNAs, featured by the covalently closed-loop structure, without 5' cap and 3' tail [5]. Due to the specific structure, circRNAs are extremely stable; and are generally distributed in the cytoplasm [6]. Numerous circRNAs were demonstrated to have important regulatory roles in human cancers, including OS [7, 8]. Derived from cyclin dependent kinase 14 (CDK14), circ_CDK14 (circBase ID: hsa_circ_0001721; location: chr7:90355880-90356126; spliced sequence length: 246 bp) was discovered to be upregulated in OS tissues [9]. However, the action mechanism of circ_CDK14 in OS progression has not been fully elucidated.

MicroRNAs (miRNAs) are short non-coding RNAs with only ~22 nucleotides in length, endowing with significant regulatory roles in cancer-related pathways [10, 11]. miRNAs could exert functions by binding to 3' untranslated region (UTR) of their target message RNAs (mRNAs), thereby regulating cell proliferation, differentiation, and metastasis [12, 13]. For example, miRNA-708 repressed OS cell proliferation while contributed to apoptosis by targeting CUL4B [14]. miR-449a and miR-424 inhibited OS cell proliferation via targeting cyclin A2 [15]. As reported, miR-520-3p was involved in dexmedetomidine-mediated inhibitory effects on OS cell proliferation and migration [16]. Here, StarBase 3.0 predicted that miR-520-3p was a possible target miRNA of circ_CDK14. Whether miR-520-3p participates in circ_CDK14-mediated OS progression needs to be clarified.

GRB2 Associated Binding Protein 1 (GAB1) is a key regulator of multiple growth factors and cytokine signaling pathways [17]. GAB1 was reported to be a tumor-promoting agent in breast cancer [18], oral squamous cell carcinoma [19], and hilar cholangiocarcinoma [20]. In OS, GAB1 was predicted to be an oncogenic driver by *Sleeping Beauty* (SB) transposon-based analysis [21]. In this study, GAB1 was forecasted to be a target mRNA of miR-520-3p by StarBase 3.0. However, the role of GAB1 in OS progression remains unclear.

Herein, the expression level of circ_CDK14 in OS was determined. Also, the functional role of circ_CDK14 in OS cell proliferation, metastasis, and tumorigenesis was explored, along with the possible mechanistic pathway.

Patients and methods

Tissue collection and cell culture. 43 pairs of OS tissues and adjacent normal tissues were collected from patients hospitalized at the Affiliated Huai'an No.1 People's Hospital of Nanjing Medical University. All of these 43 patients submitted written informed consents. All samples were kept at −80 °C until used. This permission of the Ethics Committees of the Affiliated Huai'an No.1 People's Hospital of Nanjing Medical University was obtained for conducting the current study.

Human osteoblast cell line hFOB 1.19 (ATCC® CRL-11372), OS cell lines MG63 (ATCC® CRL-1427) and SaOS-2 (ATCC® HTB-85) were purchased from the American Type Culture Collection (Manassas, VA, USA). All cells were maintained in Dulbecco's modified Eagle medium (Gibco, Grand Island, NY, USA) mixed with 10% fetal bovine serum (FBS; HyClone, Logan, UT, USA) and 1% penicillin/streptomycin (Gibco) at 37 °C in an incubator containing 5% CO_2 and 95% air.

Cell transfection. Small interference RNA (siRNA) targeting circ_CDK14 (si-circ_CDK14) and its negative control si-NC, miR-520a-3p mimic (miR-520a-3p) and its negative control miR-NC, miR-520a-3p inhibitor (anti-miR-520a-3p) and its negative control anti-miR-NC, as well as overexpression vector of GAB1 (GAB1) and pcDNA3.1 vector (pcDNA) were all supplied by RIBOBIO Co. Ltd. (Guangzhou, China). The sequences of oligonucleotides are exhibited in Table 1. Above oligonucleotides or plasmids were introduced into MG63 and SaOS-2 cells using Lipofectamine 3000 (Invitrogen, Carlsbad, CA, USA). At 48 h after transfection, cells were subjected for further assays.

Quantitative real-time PCR (qRT-PCR). In order to extract total RNA from tissue samples and cultured cells, TRIzol Reagent (Invitrogen) was applied in strict accordance with the user's manual. After detection using NanoDrop ND-1000 spectrophotometer (Thermo Fisher Scientific, Inc., Waltham, MA, USA). 1 μg RNA was reverse-transcribed into complementary DNA (cDNA) utilizing M-MLV Reverse Transcriptase (Invitrogen) or TaqMan MicroRNA Reverse Transcription Kit (Thermo Fisher Scientific, Inc.). qRT-PCR was implemented with SYBR Master Mix (Applied Biosystems, Austin, TX, USA) or miRNA-specific TaqMan MiRNA Assay Kit (Applied Biosystems). The primers involved in the qRT-PCR assay are shown in Table 2. Relative expression of genes was determined with the $2^{-\Delta\Delta Ct}$ method [22], with normalization to glyceraldehyde-3-phosphate dehydrogenase (GAPDH) or U6.

Actinomycin D treatment. This assay was carried out to assess the stability of circ_CDK14 and CDK14. Transcription inhibitor actinomycin D (2 mg/ml; Sigma-Aldrich, St. Louis, MO, USA) or dimethyl sulfoxide (DMSO; Sigma-Aldrich) was added into the culture medium of MG63 and SaOS-2 cells. At 0 h, 8 h, 16 h, or 24 h post-treatment, relative expression levels of circ_CDK14 and CDK14 were analyzed by the qRT-PCR assay.

Nuclear-cytoplasmic fractionation. This assay was employed to explore the intracellular localization of circ_CDK14. As the user's manual directed, the PARIS™ Kit (Invitrogen) was applied to isolate the nuclear and cytoplasmic fractions. In brief, MG63 and SaOS-2 cells were mixed with cell fractionation buffer and then centrifuged. The super-

Table 1. The sequences of oligonucleotides in this study.

Name	Sequence (5'–3')
si-circ_CDK14	5'-GCCCCAGCTCGATATGTGTCA-3'
si-NC	5'-AACAGTCGCGTTTGCGACTGG-3'
miR-520a-3p	5'-AAAGUGCUUCCCUUUGGACUGU-3'
miR-NC	5'-CGAUCGCAUCAGCAUCGAUUGC-3'
anti-miR-520a-3p	5'-UUUCACGAAGGGAAACCUGACA-3'
anti-miR-NC	5'-CUAACGCAUGCACAGUCGUACG-3'

Table 2. The primer sequences for qRT-PCR assay in this study.

Gene	Sequence	
	Forward (5'-3')	Reverse (5'-3')
circ_CDK14	5'-CCACTGGCAAAGAGTCACCT-3'	5'-AATTGTGTCCAGGGGTTTGA-3'
CDK14	5'-CCATACCAAGGAGACGCTGACA-3'	5'-AGACAGACCTCGCAGCAACTGA-3'
GAB1	5'-GGAAACTCTTGGCATTCAGGAGG-3'	5'-GCAGTCTGTTTCAGAAGAGGTGG-3'
GAPDH	5'-TGTTCGTCATGGGTGTGAAC-3'	5'-ATGGCATGGACTGTGGTCAT-3'
miR-520a-3p	5'-CTCAACTGGTGTCGTGGAGTCGGCAATTCAGTTGAGACAGTCCAAA-3'	5'-ACACTCCAGCTGGGAAAGTGCTTCCC-3'
U6	5'-CTCGCTTCGGCAGCACA-3'	5'-AACGCTTCACGAATTTGCGT-3'

natant was transferred to fresh RNase-free tubes. The pellet was added with cell disruption buffer for lysis. Then supernatant or lysate was treated with 2× lysis/binding solution for cytoplasmic or nuclear RNA extraction. GAPDH and U6 served as a positive control for cytoplasmic and nuclear fractions, respectively.

Flow cytometry. For cell cycle detection, propidium iodide (PI, Sigma-Aldrich) staining was carried out. After transfection, 1×10^6 MG63 and SaOS-2 cells were rinsed using PBS (Gibco), then immobilized with 70% ethanol at 4 °C overnight, followed by incubation with RNase A and PI (Sigma-Aldrich). Finally, cells were analyzed by the FACSCalibur Flow Cytometer (BD Biosciences, Franklin Lakes, NJ, USA).

For examining cell apoptosis, Annexin V-fluorescein isothiocyanate (FITC) Apoptosis Detection kit (BD Biosciences) was used. According to the manufacturer's directions, MG63 and SaOS-2 cells after transfection were harvested and stained with Annexin V-FITC for 15 min, then PI was added to incubate cells for additional 15 min. Afterward, apoptotic OS cells were monitored using a flow cytometer (BD Biosciences) equipped with Cell Quest 6.0 software (BD Biosciences). The apoptosis rate meant the percentage of Annexin V+ PI+ or PI– cells.

Methyl thiazolyl tetrazolium (MTT) assay. This assay was performed to assess cell viability. 4×10^3 transfected MG63 and SaOS-2 cells were plated on 96-well plates and maintained for 0 d, 1 d, 2 d, or 3d. Subsequently, 20 μl MTT (5 mg/ml; Sigma-Aldrich) was pipetted into each well. After incubation for another 4 h, MTT solution was discarded, and dimethyl sulfoxide was added. Finally, the optical density (OD) value at 570 nm was recorded utilizing a microplate reader (Bio-Rad, Hercules, CA, USA).

Colony formation assay. After transfection, 500 MG63 and SaOS-2 cells were plated on 6-well plates and maintained at 37 °C for 2 weeks. Generated colonies (with exceeding 50 cells) were subjected for fixation with 4% paraformaldehyde (Beyotime, Shanghai, China), stained with crystal violet (Beyotime), photographed and counted using ImageJ software (NIH, Bethesda, MD, USA).

Western blot assay. This assay was implemented referring to a previous report [23]. 50 μg protein samples were loaded onto 12% fresh sodium dodecyl sulfate-polyacrylamide gel electrophoresis (SDS-PAGE) for separation, then transferred onto polyvinylidene difluoride (PVDF) membranes (Thermo Fisher Scientific, Inc.) by wet electrophoretic transfer method. Subsequently, membranes were subjected for blockage with 5% fat-free milk at room temperature for 2 h, incubated with rabbit monoclonal primary antibody against B-cell lymphoma-2 (Bcl-2; ab32124, Abcam, Shanghai, China; 1:2000 dilution), BCL2-Associated X (Bax; ab32503, Abcam; 1:1500 dilution), cleaved PARP (ab32064, Abcam; 1:1000 dilution), GAB1 (ab133486, Abcam; 1:1000 dilution) or GAPDH (ab181602, Abcam; 1:3000 dilution) at 4 °C overnight, and further incubation with secondary antibody goat anti-rabbit IgG H&L (HRP) (ab205718, Abcam; 1:5000 dilution) at room temperature for 2 h. After visualization using enhanced chemiluminescence (ECL) detection kit (Thermo Fisher Scientific, Inc.), the intensity of protein blots was analyzed with ImageJ software, normalized to GAPDH.

Transwell assay. Transwell assay was applied to assess the migration and invasion capacities of OS cells using Transwell chambers (8 μm pores; Corning Inc., Corning, NY, USA). For migration examination, 1×10^4 transfected MG63 and SaOS-2 cells in an FBS-free medium were placed into the upper chambers. For invasion detection, 5×10^4 transfected cells in FBS-free medium were seeded into the upper chambers pre-coated with Matrigel (BD Bioscience). Meanwhile, a complete medium was added into the lower chambers. After 24 h, cells migrated or invaded through the fibronectin-coated polycarbonate membrane were immobilized with 4% polyformaldehyde, dyed with crystal violet solution, and observed under an inverted microscope (100×; Olympus, Tokyo, Japan). Five randomly chosen fields were captured and cells were counted.

Dual-luciferase reporter assay. StarBase 3.0 (http://starbase.sysu.edu.cn/) was searched to predict the target genes of circ_CDK14 and miR-520a-3p, and miR-520a-3p and GAB1 were identified as candidates, respectively. A dual-luciferase reporter assay was conducted to validate the prediction. Wide-type luciferase reporter plasmids of circ_CDK14 and GAB1 harboring the predicted binding sites, as well as mutant-type ones embracing mutant binding sites were constructed by RIBOBIO Co. Ltd. Above constructs and miR-NC or miR-520a-3p were co-transfected into MG63 and SaOS-2 cells. At 48 h post-transfection, luciferase activity was determined using a Dual-Luciferase reporter system (Beyotime).

Tumor xenograft in nude mice. This assay was conducted with the approval from the Ethics Committees of the Affiliated Huai'an No.1 People's Hospital of Nanjing Medical University. Ten BALB/c nude mice (5 weeks old, male) purchased from Shanghai SLAC Laboratory Animal Co., Ltd. (Shanghai, China) were subcutaneously inoculated with 2×10^6 MG63 cells stably transfected with sh-NC or sh-circ_CDK14 (n=5). The volume (length × width^2/2) of formed tumors was recorded once a week. 5 weeks after injection, all mice were anesthetized using pentobarbital sodium and sacrificed. Then, tumors were collected for weighing and examining gene expression.

Statistical analysis. All data were taken from at least three independent experiments, followed by statistical analysis utilizing SPSS 20.0 (SPSS Inc., Chicago, IL, USA). Data were shown as mean ± standard deviation and compared using Student's t-test or one-way analysis of variance (ANOVA) followed by Tukey's test. Correlation analysis among the expression of circ_CDK14, miR-520a-3p, and GAB1 in OS tissues was executed by Pearson's correlation analysis. A p-value <0.05 was defined as statistically significant.

Results

Circ_CDK14 was highly expressed in OS tissues and cells. In order to investigate the role of circ_CDK14 in OS development, we firstly detected the expression of circ_CDK14 in OS tissues and normal tissues. As shown in Figure 1A, circ_CDK14 was significantly upregulated in OS tissues when compared to normal tissues. And the expression of circ_CDK14 in MG63 and SaOS-2 cells was higher than that in hFOB1.19 cells (Figure 1B). We then examined the stability of circ_CDK14 and linear CDK14. After actinomycin D treatment, the half-life of circ_CDK14 was more than 24 h, but that of CDK14 was only about 12 h, suggesting that circ_CDK14 was more stable than CDK14 (Figures 1C, 1D). Nuclear-cytoplasmic fractionation revealed that circ_CDK14 mainly localized in the cytoplasm of OS cells, implying its potential to adsorb miRNAs (Figures 1E, 1F). To sum up, circ_CDK14 was a potential oncogene in OS progression.

Depletion of circ_CDK14 inhibited OS cell proliferation and metastasis but facilitated apoptosis. Afterward, series of functional assays were performed to evaluate the effects of circ_CDK14 on cellular behaviors of OS cells. MG63 and SaOS-2 cells with circ_CDK14 knockdown were successfully established by introduction with si-circ_CDK14, and cells transfected with si-NC served as control. Meanwhile, the expression of CDK14 in transfected cells was changeless (Figures 2A, 2B). As exhibited in Figures 2C and 2D, OS

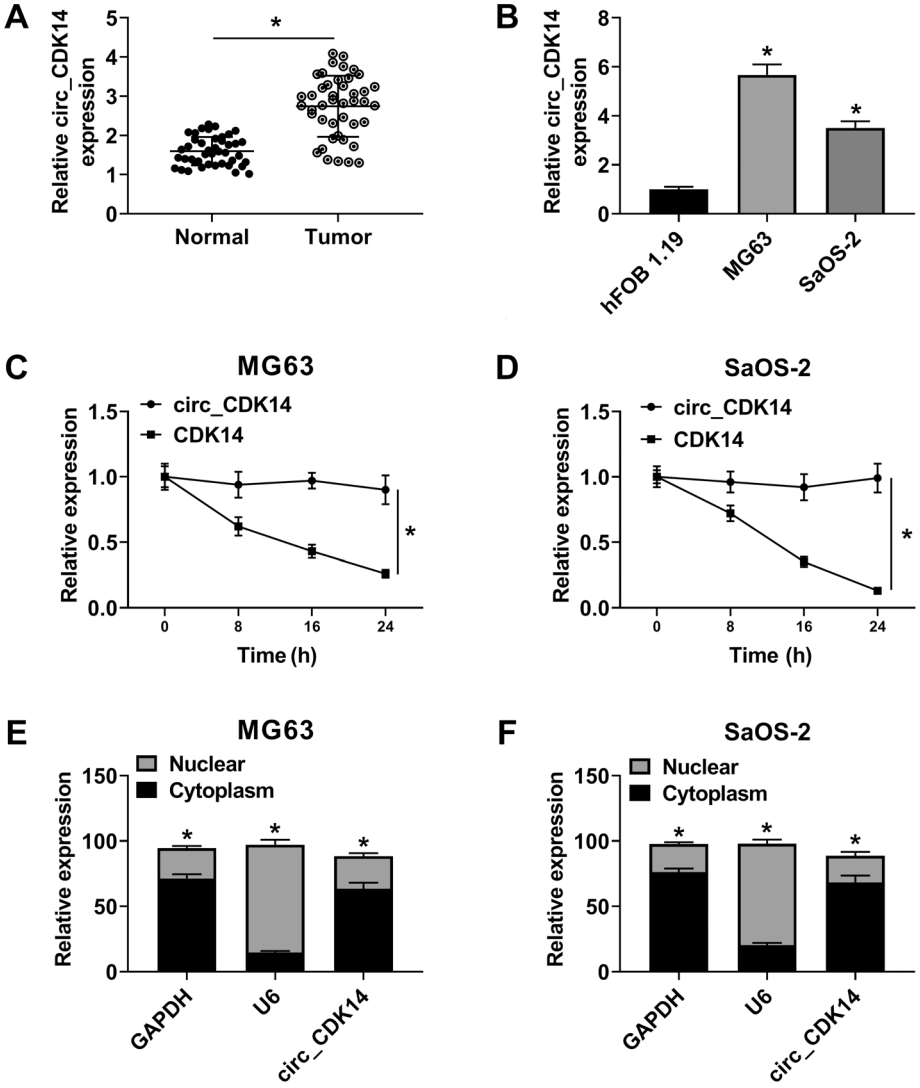

Figure 1. Circ_CDK14 was highly expressed in OS tissues and cells. A) The qRT-PCR assay for the relative expression of circ_CDK14 in OS tissues and normal tissues. B) The qRT-PCR assay for the relative expression of circ_CDK14 in hFOB1.19, MG63, and SaOS-2 cells. C, D) The qRT-PCR assay for the abundance of circ_CDK14 and CDK14 in MG63 and SaOS-2 cells treated with actinomycin D for the indicated time. E, F) Nuclear-cytoplasmic fractionation for the location of circ_CDK14 in MG63 and SaOS-2 cells. *p<0.05

cells with circ_CDK14 knockdown showed a prolonged G0/G1 stage and a shortened S stage in contrast to cells transfected with si-NC, suggesting that circ_CDK14 knockdown promoted cell cycle arrest. MTT assay showed that circ_CDK14 depletion efficiently reduced cell viability of MG63 and SaOS-2 cells (Figures 2E, 2F). Following colony formation assay proved the circ_CDK14 knockdown-induced the declined colony formation capacity of OS cells (Figure 2G).

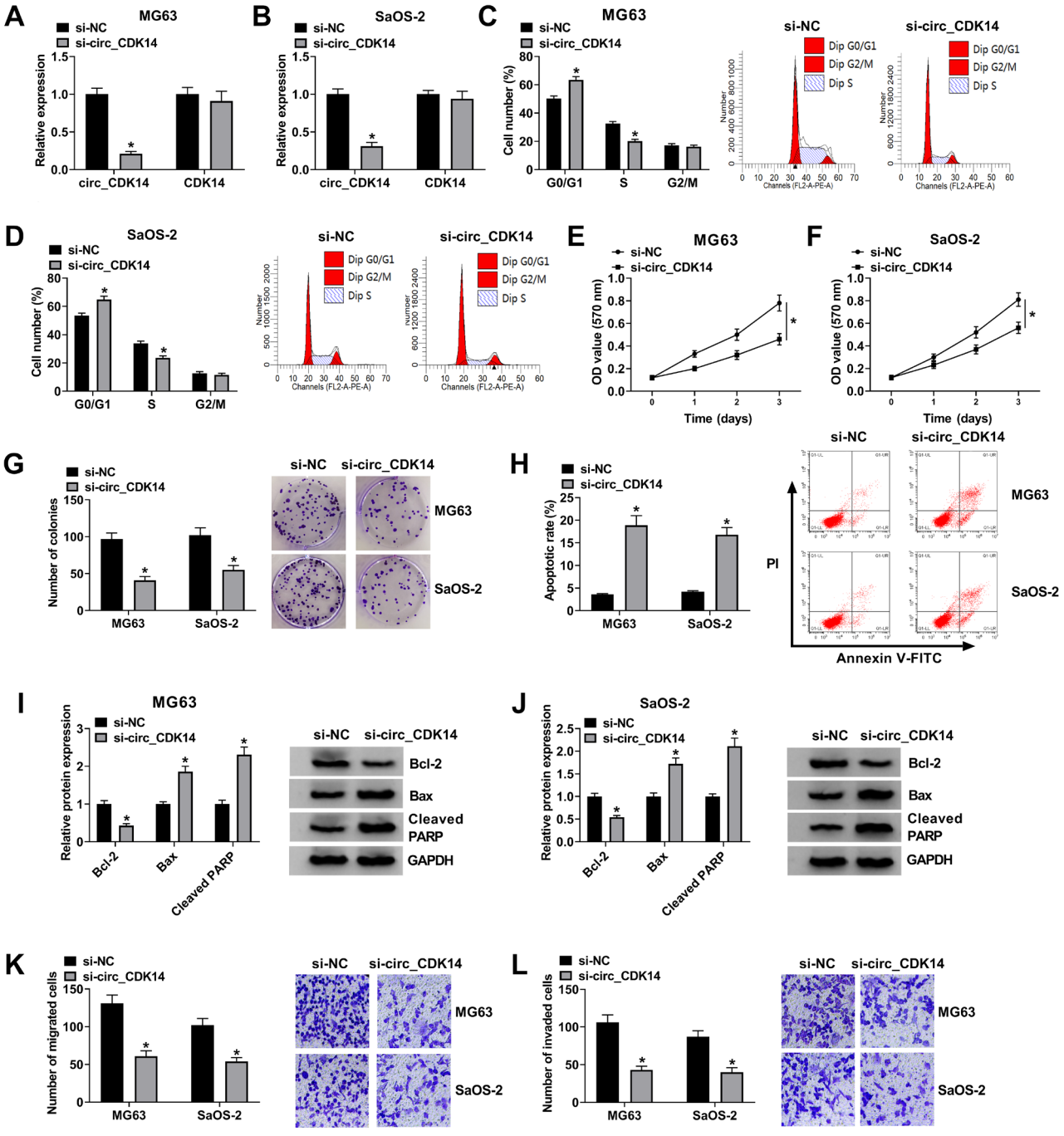

Figure 2. Depletion of circ_CDK14 inhibited OS cell proliferation and metastasis but facilitated apoptosis. MG63 and SaOS-2 cells were transfected with si-NC or si-circ_CDK14. A, B) The qRT-PCR assay for the relative expression of circ_CDK14 and CDK14 in transfected cells. C, D) Flow cytometry for the cell cycle distribution of transfected cells. E, F) MTT assay for the cell viability of transfected cells. G) Colony formation assay for the colony formation capacity of transfected cells. H) Flow cytometry for the apoptotic rate in transfected cells. I, J) Western blot assay for the protein levels of Bcl-2, Bax, and cleaved PARP in transfected cells. K, L) Transwell assay for the migration and invasion abilities of transfected cells. *p<0.05

Additionally, flow cytometry showed that silencing of circ_CDK14 apparently heightened apoptotic rate in MG63 and SaOS-2 cells (Figure 2H). Subsequently, a western blot assay was performed to detect the expression of cell apoptosis-related proteins (Bcl-2, Bax, and cleaved PARP). Obviously, circ_CDK14 knockdown decreased Bcl-2 expression and upregulated Bax and cleaved PARP levels, indicating that circ_CDK14 knockdown promoted OS cell apoptosis (Figures 2I, 2J). Moreover, the Transwell assay revealed that circ_CDK14 depletion suppressed OS cell migration and invasion (Figures 2K, 2L). Also, another siRNA (si-circ_CDK14#) also exhibited a similar effect with si-circ_CDK14 on the OS cells (Supplementary Figure S1). Taken together, circ_CDK14 knockdown suppressed cell proliferation and metastasis but promoted apoptosis of OS cells.

Circ_CDK14 acted as a sponge of miR-520a-3p. Online tool StarBase 3.0 was predicted that miR-520a-3p was a potential target miRNA of circ_CDK14. The predicted binding positions were shown in Figure 3A. Following the dual-luciferase reporter assay was performed to verify this prediction. Results suggested that compared to miR-NC, introduction of miR-520a-3p resulted in more than 60% reduction in luciferase activity of MG63 and SaOS-2 cells co-transfected with circ_CDK14-WT. No obvious change was observed in luciferase activity of MG63 and SaOS-2 cells co-transfected with circ_CDK14-MUT (Figures 3B, 3C). Furthermore, we found that circ_CDK14 knockdown upregulated miR-520a-3p expression in MG63 and SaOS-2 cells (Figure 3D). When compared with normal tissues, miR-520a-3p was downregulated in OS tissues (Figure 3E). Moreover, miR-520a-3p expression in OS tissues was negatively correlated with circ_CDK14 level ($r=-0.7643$, $p<0.0001$; Figure 3F). As expected, miR-520a-3p expression was downregulated in MG63 and SaOS-2 cells relative to hFOB1.19 cells (Figure 3G). Therefore, circ_CDK14 could target miR-520a-3p in OS cells.

Circ_CDK14 knockdown inhibited OS cell proliferation and metastasis but facilitated apoptosis by sponging miR-520a-3p. Having known that circ_CDK14 could target miR-520a-3p in OS cells, we further explored the involvement of miR-520a-3p in circ_CDK14-mediated OS development. As exhibited in Figure 4A, circ_CDK14 depletion-induced upregulation of miR-520a-3p in MG63 and SaOS-2 cells was largely weakened by miR-520a-3p inhibitor. And, circ_CDK14 knockdown-induced cell cycle arrest in OS cells was alleviated by the introduction of anti-miR-520a-3p (Figures 4B, 4C). Moreover, the aforementioned declined cell viability (Figures 4D, 4E) and colony formation capacity (Figure 4F) of MG63 and SaOS-2 cells triggered by circ_CDK14 depletion were largely relieved by miR-520a-3p inhibitor. Furthermore, circ_CDK14 knockdown induced elevated apoptotic rate (Figure 4G), downregulation of Bcl-2 protein, and upregulation of Bax and cleaved PARP proteins (Figures 4H, 4I) in MG63 and SaOS-2 cells attenuated by co-transfection of anti-miR-520a-3p. miR-520a-3p inhibition also mitigated the repressed effects of circ_CDK14 depletion on OS cell migration and invasion (Figure 4J, 4K). Collectively, the silencing of circ_CDK14 exerted anti-proliferation, anti-metastasis, and pro-apoptotic roles in OS cells by upregulating miR-520a-3p.

Figure 3. Circ_CDK14 acted as a sponge of miR-520a-3p. A) The predicted binding positions between circ_CDK14 and miR-520a-3p by StarBase 3.0. B, C) Dual-luciferase reporter assay for the luciferase activity of MG63 and SaOS-2 cells co-transfected with miR-NC or miR-520a-3p and circ_CDK14-WT or circ_CDK14-MUT. D) The qRT-PCR assay for the relative expression of miR-520a-3p in MG63 and SaOS-2 cells transfected with si-NC or si-circ_CDK14. E) The qRT-PCR assay for the relative expression of miR-520a-3p in OS tissues and normal tissues. F) Pearson's correlation analysis for the correlation between circ_CDK14 and miR-520a-3p expression in OS tissues. G) The qRT-PCR assay for the relative expression of miR-520a-3p in hFOB1.19, MG63, and SaOS-2 cells. *p<0.05

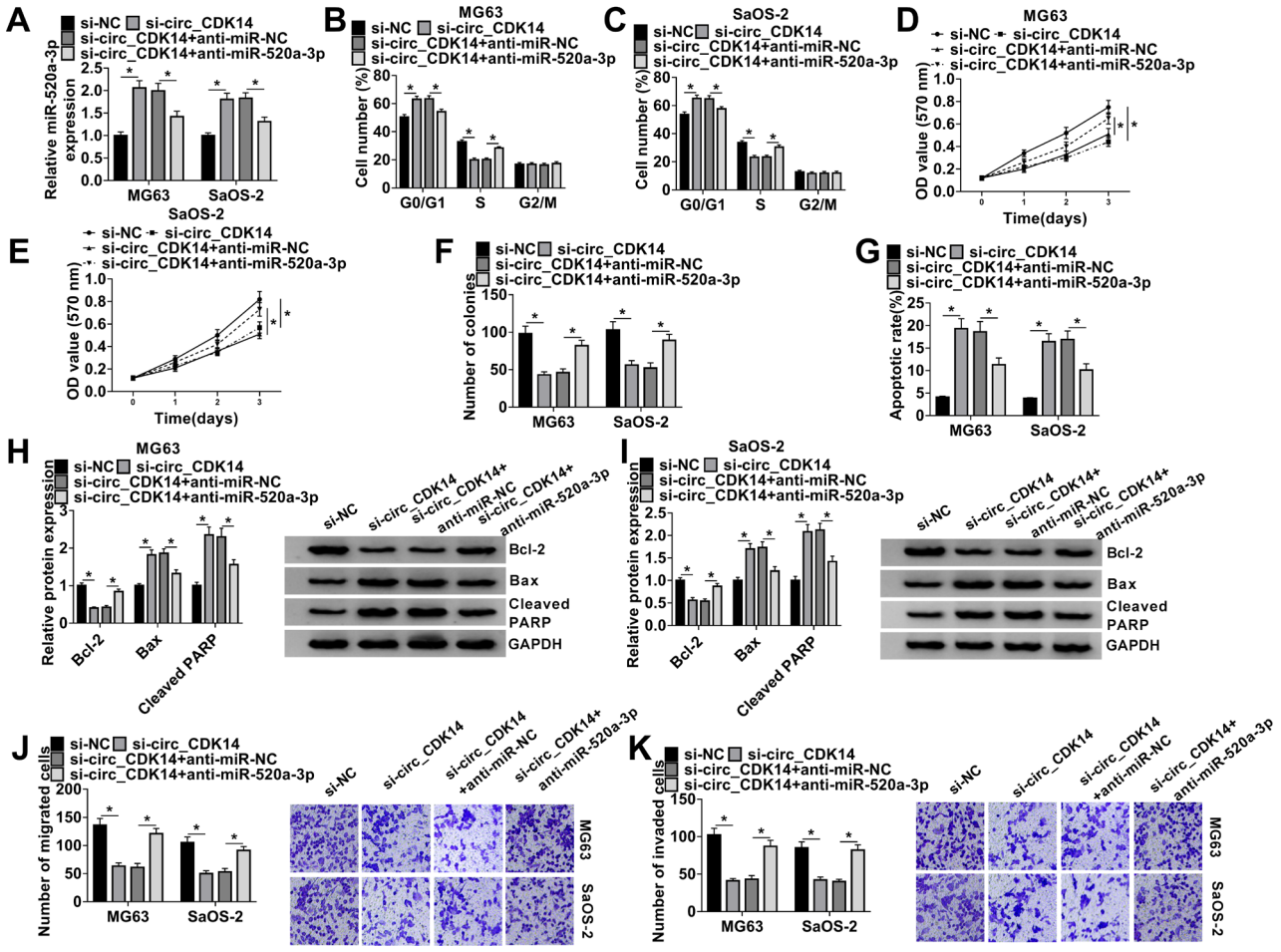

GAB1 was a direct target of miR-520a-3p. StarBase 3.0 was also applied to search the target gene of miR-520a-3p. And GAB1 3'UTR was found to have binding sites with miR-520a-3p (Figure 5A). Dual-luciferase reporter assay manifested that miR-520a-3p remarkably reduced the luciferase activity of MG63 and SaOS-2 cells co-transfected with GAB1 3'UTR-WT but it had no significant effect on that of cells co-transfected with GAB1 3'UTR-MUT (Figures 5B, 5C). As shown in Figure 5D, miR-520a-3p expression was obviously increased in MG63 and SaOS-2 cells due to transfection with miR-520a-3p; and miR-520a-3p expression was decreased in cells transfected with anti-miR-520a-3p. Furthermore, we found that miR-520a-3p overexpression reduced GAB1 mRNA and protein levels. On the contrary, downregulated miR-520a-3p enhanced GAB1 expression (Figures 5E, 5F). Moreover, the mRNA (Figure 5G) and protein (Figure 5H) levels of GAB1 in OS tissues were higher than those in normal tissues. GAB1 mRNA expression in OS tissues was inversely correlated with miR-520a-3p expression ($r=-0.5668$, $p<0.0001$; Figure 5I), while positively correlated with circ_CDK14 level ($r=0.7818$, $p<0.0001$; Figure 5J). Similarly, GAB1 expression was upregulated in MG63 and SaOS-2 cells relative to hFOB1.19 cells (Figures 5K, 5L). Therefore, miR-520a-3p targeted GAB1 and negatively regulated GAB1 expression OS cells.

miR-520a-3p could repress OS cell proliferation and metastasis, while contributes to apoptosis by targeting GAB1. We then investigated the co-effects of miR-520a-3p and GAB1 on OS development. As exhibited in Figures 6A and 6B, miR-520a-3p overexpression significantly inhibited GAB1 expression, which was weakened by transfection with GAB1. Furthermore, miR-520a-3p-induced cell cycle arrest

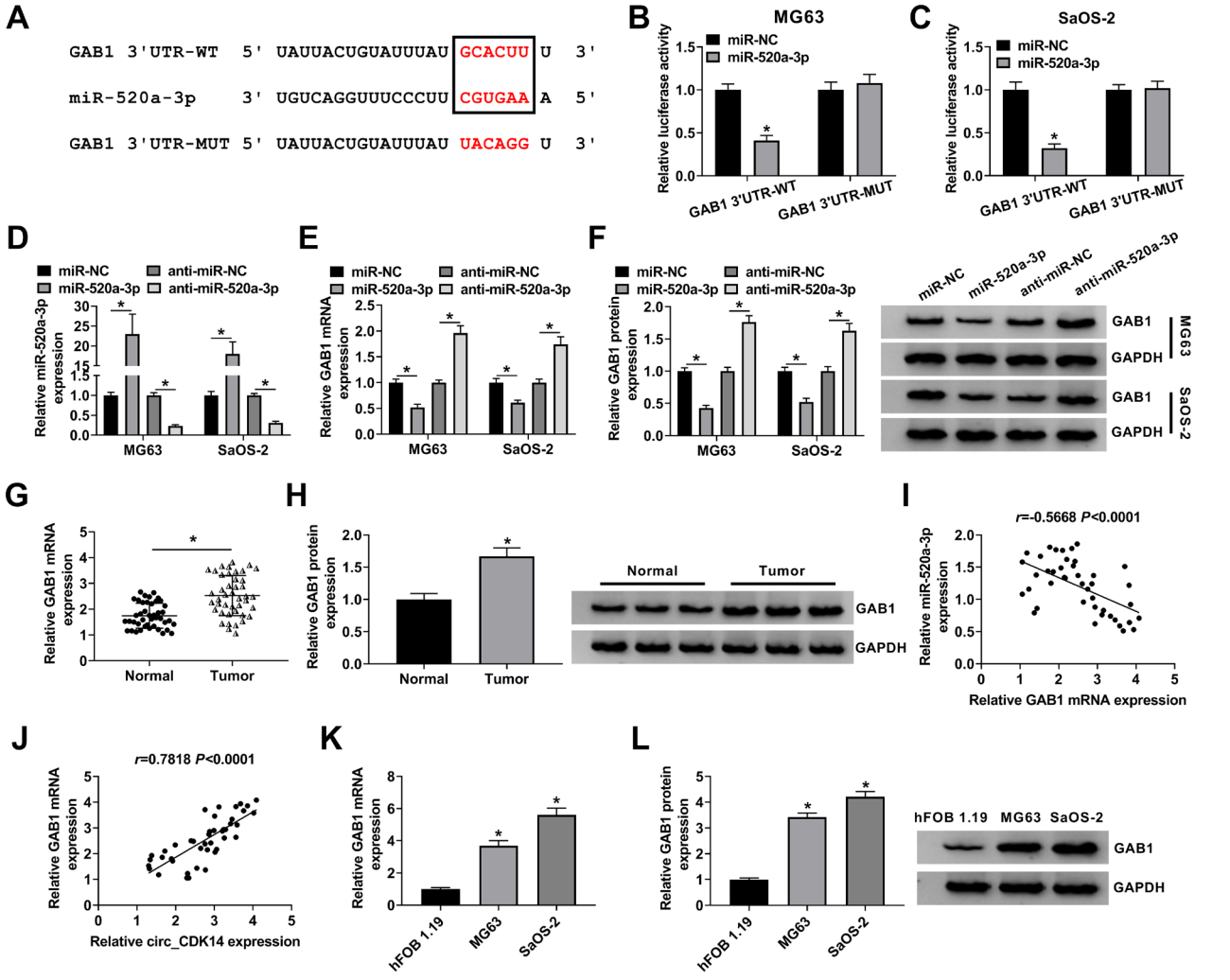

Figure 5. GAB1 was a direct target of miR-520a-3p. A) The predicted binding sites between miR-520a-3p and GAB1 3'UTR by StarBase 3.0. B, C) A dual-luciferase reporter assay for the luciferase activity of MG63 and SaOS-2 cells co-transfected with miR-NC or miR-520a-3p and GAB1 3'UTR-WT or GAB1 3'UTR-MUT. D) The qRT-PCR assay for the relative expression of miR-520a-3p in MG63 and SaOS-2 cells transfected with miR-NC, miR-520a-3p, anti-miR-NC, or anti-miR-520a-3p. E) The qRT-PCR assay for the relative expression of GAB1 mRNA in MG63 and SaOS-2 cells transfected with miR-NC, miR-520a-3p, anti-miR-NC, or anti-miR-520a-3p. F) Western blot assay for the relative expression of GAB1 protein in MG63 and SaOS-2 cells transfected with miR-NC, miR-520a-3p, anti-miR-NC, or anti-miR-520a-3p. G) The qRT-PCR assay for the relative expression of GAB1 mRNA in OS tissues and normal tissues. H) Western blot assay for the relative expression of GAB1 protein in OS tissues and normal tissues. I) Pearson's correlation analysis for the correlation between miR-520a-3p and GAB1 mRNA expression in OS tissues. J) Pearson's correlation analysis for the correlation between circ_CDK14 and GAB1 mRNA expression in OS tissues. K) The qRT-PCR assay for the relative expression of GAB1 mRNA in hFOB1.19, MG63, and SaOS-2 cells. L) Western blot assay for the relative expression of GAB1 protein in hFOB1.19, MG63, and SaOS-2 cells. *p<0.05

(Figures 6C, 6D), reduced cell viability (Figures 6E, 6F), declined colony formation capacity (Figure 6G), elevated apoptotic rate (Figure 6H), downregulated Bcl-2 and upregulated Bax and cleaved PARP (Figures 6I, 6J), and inhibited cell migration and invasion (Figures 6K, 6L) in MG63 and SaOS-2 cells when were all attenuated by introduced GAB1. Therefore, miR-520a-3p inhibited OS progression by downregulating GAB1.

Circ_CDK14 knockdown blocked OS tumor growth *in vivo*. To clarify the effect of sh-circ_CDK14 on the OS growth *in vivo*, MG63 cells stably transfected with sh-NC or sh-circ_CDK14 were subcutaneously injected into nude mice. Compared to the sh-NC group, smaller size and lower weight were observed in generated tumors of the sh-circ_CDK14 group (Figures 7A, 7B, Supplementary Figure S2). The qRT-PCR assay showed that circ_CDK14 (Figure 7C) and GAB1 mRNA (Figure 7E) were downregulated, while miR-520a-3p (Figure 7D) was upregulated in tumors of the sh-circ_CDK14 group. Western blot assay results revealed that GAB1 protein was also downregulated in the sh-circ_CDK14 group (Figure 7F). The above results suggested that silencing of circ_CDK14 could inhibit OS growth *in vivo*.

Discussion

Non-coding RNAs have been observed to participate in the physiological and pathological processes of OS, including circRNAs and miRNAs [24]. Additionally, non-coding RNAs could act as diagnostic or prognostic biomarkers to indicate the disease status of OS patients [25]. In this study, we found that circ_CDK14 could facilitate OS development by regulating the miR-520a-3p/GAB1 pathway, at least in part.

Circ_CDK14, also named hsa_circ_0001721, was found to be upregulated in OS tissues in contrast to matched normal tissues, demonstrated by circRNAs expression profiles analysis and qRT-PCR assay [9]. Li et al. also detected the upregulation of circ_CDK14 in OS tissue samples and cells. And circ_CDK14 expression was correlated with bigger tumor size and advanced WHO grade. In addition, circ_CDK14 exerted oncogenic roles in OS progression by sponging miR-569 and miR-599 [26]. Here, we also found that circ_CDK14 expression was highly enriched in OS tissues and cells. Functionally, silencing of circ_CDK14 inhibited proliferation and metastasis of OS cells *in vitro*, as well as hampered tumor growth *in vivo*, highlighting that circ_CDK14 was an oncogene in OS.

Mechanistically, circRNAs could serve as sponges of miRNAs to affect the proliferation and apoptosis of OS cells [27]. In this study, miR-520a-3p was validated to be a target miRNA of circ_CDK14. Previous literature revealed that miR-520a-3p functioned as a tumor-suppressor in colorectal cancer by regulating EGFR expression [28]. Li et al. alleged that miR-520a-3p exerted anti-proliferation and anti-metastasis roles in breast cancer cells through the negative regulation on CCND1 and CD44 expression [29]. Moreover, miR-520a-3p could also inhibit non-small cell lung cancer cell growth and metastasis, through modulating the PI3K/AKT/mTOR signaling pathway [30]. The tumor-suppressor role of miR-520a-3p was also observed in gastric cancer [31] and papillary thyroid cancer [32]. Wang et al. first demonstrated the functional role of miR-520a-3p in OS. miR-520-3p

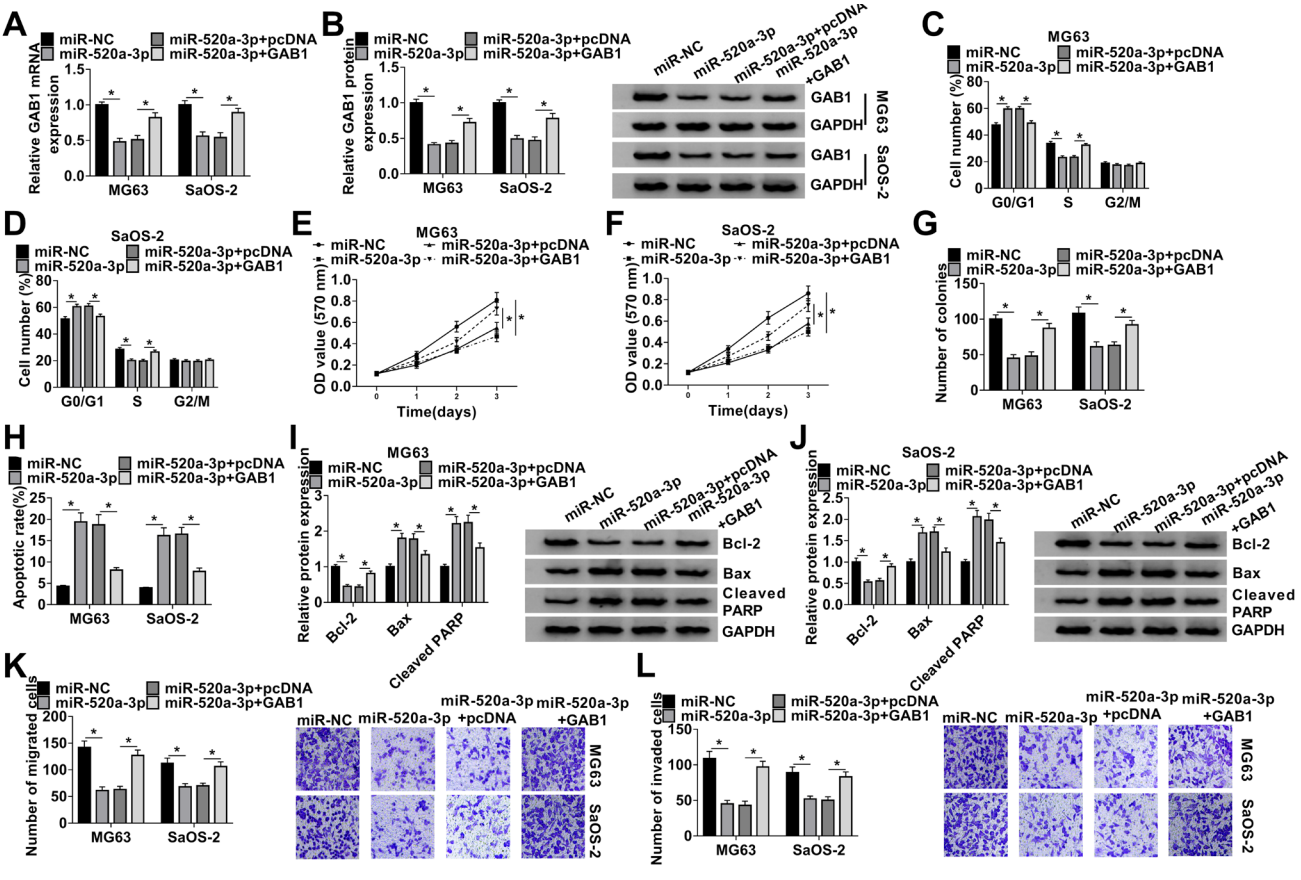

Figure 6. miR-520a-3p could repress OS cell proliferation and metastasis, while contributes to apoptosis by targeting GAB1. MG63 and SaOS-2 cells were transfected with miR-NC, miR-520a-3p, miR-520a-3p+pcDNA, or miR-520a-3p+GAB1. A) The qRT-PCR assay for the relative expression of GAB1 mRNA in transfected cells. B) Western blot assay for the relative expression of GAB1 protein in transfected cells. C, D) Flow cytometry for the cell cycle distribution of transfected cells. (E and F) MTT assay for the cell viability of transfected cells. G) Colony formation assay for the colony formation capacity of transfected cells. H) Flow cytometry for the apoptotic rate in transfected cells. I, J) Western blot assay for the protein levels of Bcl-2, Bax, and cleaved PARP in transfected cells. K, L) Transwell assay for the migration and invasion abilities of transfected cells. *p<0.05

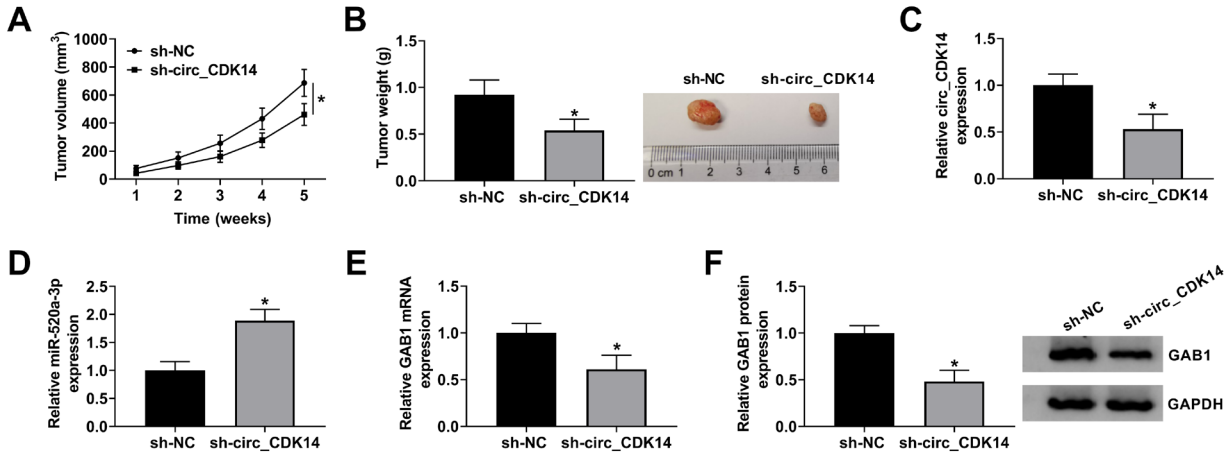

Figure 7. Circ_CDK14 knockdown blocked OS tumor growth *in vivo*. MG63 cells stably expressing sh-NC or sh-circ_CDK14 were subcutaneously injected into nude mice. A) Tumor volume measured once a week. B) Tumor weight measured 5 weeks post-injection. C–E) The qRT-PCR assay for the relative expression of circ_CDK14 (C), miR-520a-3p (D), and GAB1 mRNA (E) in generated tumors. F) Western blot assay for the relative expression of GAB1 protein in generated tumors. *p<0.05

could target AKT1 to repress OS cell proliferation and migration, acting as a tumor-suppressor [16]. From our data, miR-520a-3p was downregulated in OS tissues and cells. The introduction of miR-520a-3p suppressed OS cell proliferation and metastasis, while promoted cell apoptosis, consistent with the previous report. Furthermore, miR-520a-3p inhibition largely relieved the circ_CDK14 knockdown-mediated inhibitor impact on OS cell proliferation and metastasis. Taken together, circ_CDK14 knockdown might suppress OS development via targeting miR-520a-3p.

Accumulating circRNA-miRNA-mRNA networks have been identified to be closely associated with pathogenesis, progression, and prognosis of OS [33]. We tried to establish a ceRNA network in this project. Herein, GAB1 was confirmed as a target mRNA of miR-520a-3p in OS cells. Former research manifested that GAB1 was associated with various human cancers, serving as a target gene of miRNAs. For example, miR-383 blocked pancreatic carcinoma development by targeting GAB1 [34]. Through directly targeting GAB1, miRNA-200a inhibited hepatocellular carcinoma cell metastasis [35]. In addition, the tumor-suppressor property of miRNA-590-5p in non-small cell lung cancer was attributed to the downregulation of GAB1 expression [36]. However, the role of GAB1 in OS has not been disclosed to our knowledge. The current study revealed that GAB1 expression was upregulated in OS tissues and cells. And GAB1 overexpression could weaken miR-520a-3p induced OS cell proliferation and metastasis inhibition. Taken together, circ_CDK14/miR-520a-3p/GAB1 axis had important role in OS progression.

In conclusion, our study identified circ_CDK14 as a potential OS promoting gene. Also, circ_CDK14 knockdown repressed OS cell proliferation, metastasis, and tumorigenesis by modulating the miR-520a-3p/GAB1 pathway, at least in part. Taken together, this study highlighted a novel potential therapeutic target for OS.

Supplementary information is available in the online version of the paper.

References

[1] MOORE DD, LUU HH. Osteosarcoma. Cancer Treat Res 2014; 162: 65–92. https://doi.org/10.1007/978-3-319-07323-1_4

[2] OTTAVIANI G, JAFFE N. The epidemiology of osteosarcoma. Cancer Treat Res 2009; 152: 3–13. https://doi.org/10.1007/978-1-4419-0284-9_1

[3] LUETKE A, MEYERS PA, LEWIS I, JUERGENS H. Osteosarcoma treatment – where do we stand? A state of the art review. Cancer Treat Rev 2014; 40: 523–532. https://doi.org/10.1016/j.ctrv.2013.11.006

[4] POSTHUMADEBOER J, WITLOX MA, KASPERS GJ, VAN ROYEN BJ. Molecular alterations as target for therapy in metastatic osteosarcoma: a review of literature. Clin Exp Metastasis 2011; 28: 493–503. https://doi.org/10.1007/s10585-011-9384-x

[5] CHEN LL, YANG L. Regulation of circRNA biogenesis. RNA Biol 2015; 12: 381–388. https://doi.org/10.1080/15476286.2015.1020271

[6] CHEN LL. The biogenesis and emerging roles of circular RNAs. Nat Rev Mol Cell Biol 2016; 17: 205–211. https://doi.org/10.1038/nrm.2015.32

[7] DONG Y, HE D, PENG Z, PENG W, SHI W et al. Circular RNAs in cancer: an emerging key player. J Hematol Oncol 2017; 10: 2. https://doi.org/10.1186/s13045-016-0370-2

[8] WANG C, REN M, ZHAO X, WANG A, WANG J. Emerging Roles of Circular RNAs in Osteosarcoma. Med Sci Monit 2018; 24: 7043–7050. https://doi.org/10.12659/msm.912092

[9] ZHOU X, NATINO D, QIN Z, WANG D, TIAN Z et al. Identification and functional characterization of circRNA-0008717 as an oncogene in osteosarcoma through sponging miR-203. Oncotarget 2018; 9: 22288–22300. https://doi.org/10.18632/oncotarget.23466

[10] HAMMOND SM. An overview of microRNAs. Adv Drug Deliv Rev 2015; 87: 3–14. https://doi.org/10.1016/j.addr.2015.05.001

[11] JANSSON MD, LUND AH. MicroRNA and cancer. Mol Oncol 2012; 6: 590–610. https://doi.org/10.1016/j.molonc.2012.09.006

[12] ZHANG C, WAN J, LONG F, LIU Q, HE H. Identification and validation of microRNAs and their targets expressed in osteosarcoma. Oncol Lett 2019; 18: 5628–5636. https://doi.org/10.3892/ol.2019.10864

[13] WANG J, LIU S, SHI J, LI J, WANG S et al. The Role of miRNA in the Diagnosis, Prognosis, and Treatment of Osteosarcoma. Cancer Biother Radiopharm 2019; 34: 605–613. https://doi.org/10.1089/cbr.2019.2939

[14] CHEN G, ZHOU H. MiRNA-708/CUL4B axis contributes into cell proliferation and apoptosis of osteosarcoma. Eur Rev Med Pharmacol Sci 2018; 22: 5452–5459. https://doi.org/10.26355/eurrev_201809_15805

[15] SHEKHAR R, PRIYANKA P, KUMAR P, GHOSH T, KHAN MM et al. The microRNAs miR-449a and miR-424 suppress osteosarcoma by targeting cyclin A2 expression. J Biol Chem 2019; 294: 4381–4400. https://doi.org/10.1074/jbc.RA118.005778

[16] WANG X, XU Y, CHEN X, XIAO J. Dexmedetomidine Inhibits Osteosarcoma Cell Proliferation and Migration, and Promotes Apoptosis by Regulating miR-520a-3p. Oncol Res 2018; 26: 495–502. https://doi.org/10.3727/096504017x14982578608217

[17] ITOH M, YOSHIDA Y, NISHIDA K, NARIMATSU M, HIBI M et al. Role of Gab1 in heart, placenta, and skin development and growth factor- and cytokine-induced extracellular signal-regulated kinase mitogen-activated protein kinase activation. Mol Cell Biol 2000; 20: 3695–3704. https://doi.org/10.1128/mcb.20.10.3695-3704.2000

[18] WANG X, PENG J, YANG Z, ZHOU PJ, AN N et al. Elevated expression of Gab1 promotes breast cancer metastasis by dissociating the PAR complex. J Exp Clin Cancer Res 2019; 38: 27. https://doi.org/10.1186/s13046-019-1025-2

[19] XU L, LI J, KUANG Z, KUANG Y, WU H. Knockdown of Gab1 Inhibits Cellular Proliferation, Migration, and Invasion in Human Oral Squamous Carcinoma Cells. Oncol Res 2018; 26: 617–624. https://doi.org/10.3727/096504017x15043589260618

[20] SANG H, LI T, LI H, LIU J. Down-regulation of Gab1 inhibits cell proliferation and migration in hilar cholangiocarcinoma. PLoS One 2013; 8: e81347. https://doi.org/10.1371/journal.pone.0081347

[21] MORIARITY BS, OTTO GM, RAHRMANN EP, RATHE SK, WOLF NK et al. A Sleeping Beauty forward genetic screen identifies new genes and pathways driving osteosarcoma development and metastasis. Nat Genet 2015; 47: 615–624. https://doi.org/10.1038/ng.3293

[22] LIVAK KJ, SCHMITTGEN TD. Analysis of relative gene expression data using real-time quantitative PCR and the 2(–Delta Delta C(T)) Method. Methods 2001; 25: 402–408. https://doi.org/10.1006/meth.2001.1262

[23] ZHANG H, WANG X, HU B, ZHANG F, WEI H et al. Circular RNA ZFR accelerates non-small cell lung cancer progression by acting as a miR-101-3p sponge to enhance CUL4B expression. Artif Cells Nanomed Biotechnol 2019; 47: 3410–3416. https://doi.org/10.1080/21691401.2019.1652623

[24] WANG C, JING J, CHENG L. Emerging roles of non-coding RNAs in the pathogenesis, diagnosis and prognosis of osteosarcoma. Invest New Drugs 2018; 36: 1116–1132. https://doi.org/10.1007/s10637-018-0624-7

[25] BOTTI G, GIORDANO A, FEROCE F, DE CHIARA AR, CANTILE M. Noncoding RNAs as circulating biomarkers in osteosarcoma patients. J Cell Physiol 2019; 234: 19249–19255. https://doi.org/10.1002/jcp.28744

[26] LI L, GUO L, YIN G, YU G, ZHAO Y et al. Upregulation of circular RNA circ_0001721 predicts unfavorable prognosis in osteosarcoma and facilitates cell progression via sponging miR-569 and miR-599. Biomed Pharmacother 2019; 109: 226–232. https://doi.org/10.1016/j.biopha.2018.10.072

[27] ZHANG Y, LI J, WANG Y, JING J, LI J. The Roles of Circular RNAs in Osteosarcoma. Med Sci Monit 2019; 25: 6378–6382. https://doi.org/10.12659/msm.915559

[28] ZHANG R, LIU R, LIU C, NIU Y, ZHANG J et al. A Novel Role for MiR-520a-3p in Regulating EGFR Expression in Colorectal Cancer. Cell Physiol Biochem 2017; 42: 1559–1574. https://doi.org/10.1159/000479397

[29] LI J, WEI J, MEI Z, YIN Y, LI Y et al. Suppressing role of miR-520a-3p in breast cancer through CCND1 and CD44. Am J Transl Res 2017; 9: 146–154. PMID: 28123641

[30] LV X, LI CY, HAN P, XU XY. MicroRNA-520a-3p inhibits cell growth and metastasis of non-small cell lung cancer through PI3K/AKT/mTOR signaling pathway. Eur Rev Med Pharmacol Sci 2018; 22: 2321–2327. https://doi.org/10.26355/eurrev_201804_14822

[31] SU H, REN F, JIANG H, CHEN Y, FAN X. Upregulation of microRNA-520a-3p inhibits the proliferation, migration and invasion via spindle and kinetochore associated 2 in gastric cancer. Oncol Lett 2019; 18: 3323–3330. https://doi.org/10.3892/ol.2019.10663

[32] BI CL, ZHANG YQ, LI B, GUO M, FU YL. MicroRNA-520a-3p suppresses epithelial-mesenchymal transition, invasion, and migration of papillary thyroid carcinoma cells via the JAK1-mediated JAK/STAT signaling pathway. J Cell Physiol 2019; 234: 4054–4067. https://doi.org/10.1002/jcp.27199

[33] QIU Y, PU C, LI Y, QI B. Construction of a circRNA-miRNA-mRNA network based on competitive endogenous RNA reveals the function of circRNAs in osteosarcoma. Cancer Cell Int 2020; 20: 48. https://doi.org/10.1186/s12935-020-1134-1

[34] SU QL, ZHAO HJ, SONG CF, ZHAO S, TIAN ZS et al. MicroRNA-383 suppresses pancreatic carcinoma development via inhibition of GAB1 expression. Eur Rev Med Pharmacol Sci 2019; 23: 10729–10739. https://doi.org/10.26355/eurrev_201912_19774

[35] WANG J, SONG W, SHEN W, YANG X, SUN W et al. MicroRNA-200a Suppresses Cell Invasion and Migration by Directly Targeting GAB1 in Hepatocellular Carcinoma. Oncol Res 2017; 25: 1–10. https://doi.org/10.3727/096504016x14685034103798

[36] XU BB, GU ZF, MA M, WANG JY, WANG HN. MicroRNA-590-5p suppresses the proliferation and invasion of non-small cell lung cancer by regulating GAB1. Eur Rev Med Pharmacol Sci 2018; 22: 5954–5963. https://doi.org/10.26355/eurrev_201809_15926

https://doi.org/10.4149/neo_2021_201206N1319

Depletion of circRNA circ_CDK14 inhibits osteosarcoma progression by regulating the miR-520a-3p/GAB1 axis

Peng-Fei WU[1], Xiao-Ming TANG[1], Hai-Lang SUN[1], Hai-Tao JIANG[1], Jian MA[1], Ying-Hui KONG[2,*]

Supplementary Information

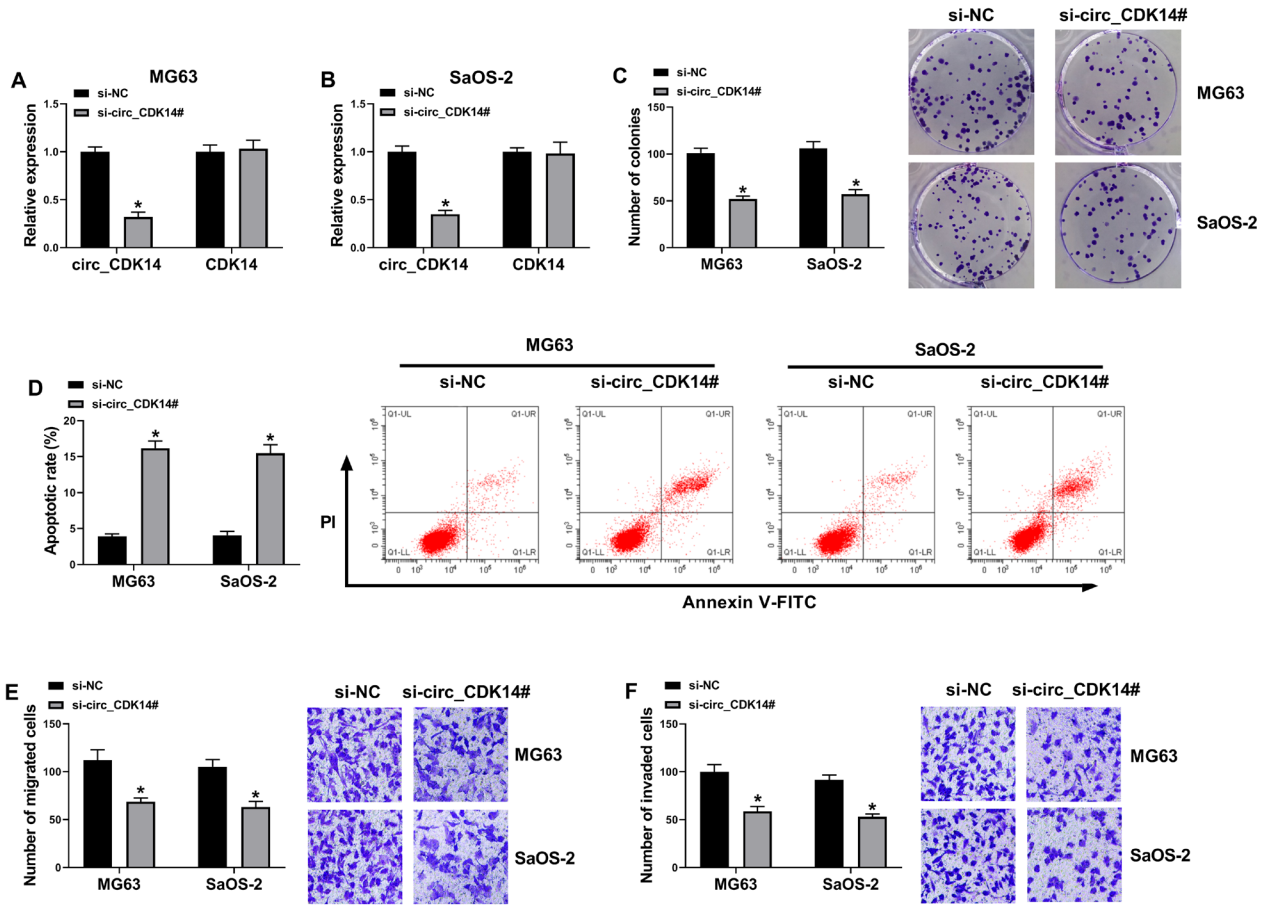

Supplementary Figure S1. The effect of another siRNA of circ_CDK14 (si-circ_CDK14#) on OS cells. MG63 and SaOS-2 cells were transfected with si-NC or si-circ_CDK14#. A, B) QRT-PCR assay for the relative expression of circ_CDK14 and CDK14 in transfected cells. C) Colony formation assay for the colony formation capacity of transfected cells. D) Flow cytometry for the apoptotic rate in transfected cells. E, F) Transwell assay for the migration and invasion abilities of transfected cells. *p<0.05

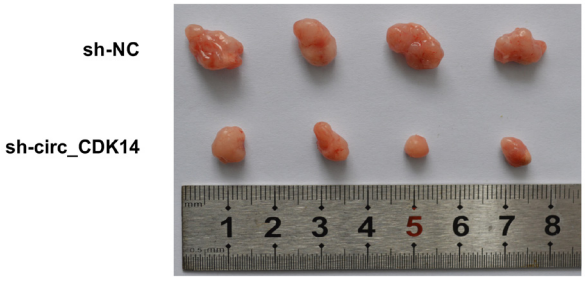

Supplementary Figure S2. The picture of tumors in nude mice.